A new instability index for unstable mode selection in squeal prediction by complex eigenvalue analysis

J. Brunetti[a,b,*], F. Massi[c,1], W. D'Ambrogio[b], Y. Berthier[a,1]

[a] *LaMCoS, Contacts and Structural Mechanics Laboratory, Université de Lyon, CNRS, INSA-Lyon, UMR 5259, 20 rue des Sciences, F-69621, Villeurbanne, France.*
[b] *DIIIE, Department of Industrial Engineering Information and Economy, Università dell'Aquila, Via G. Gronchi 18, I-67100 L'Aquila, Italy*
[c] *DIMA, Department of Mechanical and Aerospace Engineerig, Università di Roma "La Sapienza", Via Eudossiana, 18, 00184 Roma, Italy*
[d] *InTrig, International Tribology Group, Villeurbanne, France*

Abstract

During these last decades the modal instability of systems, generated by frictional contact forces, has been the subject of a huge amount of works in friction induced vibration literature. Linear and nonlinear numerical analyses have been largely investigated to predict and reproduce squeal vibrations. While nonlinear transient analysis needs large computational efforts, results of Complex Eigenvalue Analysis (CEA) suffer from an over-prediction issue and it is not able to predict correctly the mode that will become effectively unstable in case of several unstable eigenvalues. Because the CEA has been adopted as an efficient tool for brake design, a more reliable index is here proposed, from the CEA outputs and energetic considerations, to identify the mode that will become effectively unstable. A modular lumped model is developed to reproduce friction induced vibrations. The use of the eigenvalue real part, as discriminant of the system instability, is here combined with information coming from the eigenvectors, projected on the equilibrium position, to account for the energy flows involved in the squeal phenomena. This approach allows to define a Modal Absorption Index (MAI). The MAI allows for comparing unstable modes of the same system and is applied in this paper to predict, by CEA outputs, the unstable mode that will effectively result in squeal vibrations.

1. Introduction

In the analysis of Friction-Induced Vibrations (FIV) issues [1], particular emphasis has been dedicated to the unstable vibrations [2, 3]. In fact, the severe operating conditions generated by this phenomena on the mechanical systems, i.e. the high amplitude vibrations often associated to noisy sound emissions, tickled, for instance, the research on the brake squeal [4, 5] and on the hip endoprosthesis squeaking [6, 7].

This unstable behavior was originally attributed to a discrete or continuous variation of the friction coefficient with speed (velocity-slope) [8, 9]. Nowadays the idea, initially proposed by Spurr [10], that the instability can be "geometrically induced" and can be reached also with a constant friction coefficient is currently accepted. Hence, the friction force can be expressed as a follower force [11] and friction-induced vibrations are in this case very similar, from a mathematical point of view, to the flow-induced vibrations and to the flutter instability [12].

In this framework the Complex Eigenvalue Analysis (CEA) represents a fundamental tool to evaluate the stability of a mechanical system with frictional contacts, and this approach is widely used in the design and optimization process of brake systems, to avoid or at least reduce the squeal occurrence. Nevertheless,

*Corresponding author
Email addresses: jacopo.brunetti@insa-lyon.fr (J. Brunetti), francesco.massi@uniroma1.it (F. Massi), walter.dambrogio@univaq.it (W. D'Ambrogio), yves.berthier@insa-lyon.fr (Y. Berthier)

Preprint, published in *Journal of Sound and Vibrations* ***377*** *(2016), 106-122*

results from CEA provide an over-prediction of the possible unstable modes, and it is currently impossible to predict which one of the possible unstable modes will actually dominate the transient behavior.

Even if non-linear semi-analytic approaches allow to reproduce the transient behavior (i.e. amplitude of vibration) of reduced order and simplified models, in case of a single unstable mode of the system [13, 14], a full model transient analysis is required in case of multi-instabilities predicted by the CEA [15–17] to find the mode that is actually excited and the amplitude of the limit-cycle vibration.

Recently, energy approaches have been developed to evaluate the "feed-in" energy in unstable friction-induced vibrations [18, 19]. For the first time, not only the eigenvalue information but also the eigenvectors, resulting from the CEA, are used to evaluate the capability of each unstable mode to inject energy from the contact interface into the bulk of the system, as an additional information to the propensity for the instability.

In this paper a new instability index, the Modal Absorption Index (MAI) is defined; the main advantage of the new index is the possibility of comparing the capability of each unstable mode of the system to absorb energy from the contact interface; where a multi-instabilities configuration is predicted by the CEA, the new index allows for predicting the unstable mode selection occurring in the transient response of the mechanical system. The comparison between several modes was made possible by the projection of the static equilibrium position on the complex modal base. By this way it is possible to estimate the actual energy absorption due to the wide-band excitation generated at the frictional contact. Similar approaches are used in the seismic analysis of civil structures to evaluate the significance of the vibration modes, i.e. the capability of each mode to be excited by a base excitation [20].

In this paper a modular lumped model is developed to reproduce the friction-induced vibrations. The use of a lumped model allows for a fast integration of the transient solution. The performance of this new instability index have been verified for different system configurations and several operating conditions, showing a good agreement between the predicted (by the MAI index from CEA) and the simulated (by transient analysis) unstable behavior.

2. Mechanical system and numerical tools

2.1. A periodic modular lumped model

A lumped model (LM) composed of masses m connected by springs k and viscous dampers c has been developed to study the friction-induced vibrations on a simple mechanical system (cf. Fig. 1). The model is composed of both masses that are in frictional contact with rigid sliders and masses that are not in contact with the sliders, but linked to the adjacent masses. Furthermore, a static pre-load displacement δ can be applied at the upper end of the springs k_3^i, allowing for the introduction of a contact pre-load. The masses in contact with the sliders are able to switch among the different contact states (Sliding-Sticking-Detachment). The presence of both masses directly involved in the contact and masses that are not in contact, allows consideration of both the bulk and the surface behavior of a system with frictional contacts. In fact, the strong coupling between the surface behavior and the dynamic response of the system is considered to be of main importance for friction induced vibration issues [21–30].

The proposed LM is composed of single modules (i), each one composed of two masses (m_1^i and m_2^i in Fig. 1), the connecting stiffnesses and dampers ($k_{3:6}^i$ and $c_{3:6}^i$) and the respective boundary conditions (δ^i, v^i and θ^i). The module is repeated (N) times and the different modules are connected each other via stiffnesses and dampers ($k_{1:2}^i$ and $c_{1:2}^i$). Furthermore, a periodicity condition is imposed between the last (N) and the first (1) module.

The periodicity allows to account for the double modes, that are generally due to the symmetry of a system [17]. On the other hand, the modularity permits a rapid variation of the number of degrees of freedom and consequently of the system complexity. Moreover, the presence of multiple contact points reproduces, even if in a discrete way, the distribution of the contact stresses and tangential velocity over an extended contact surface, and their contribution to the exchange and dissipate energy during friction induced vibrations [31].

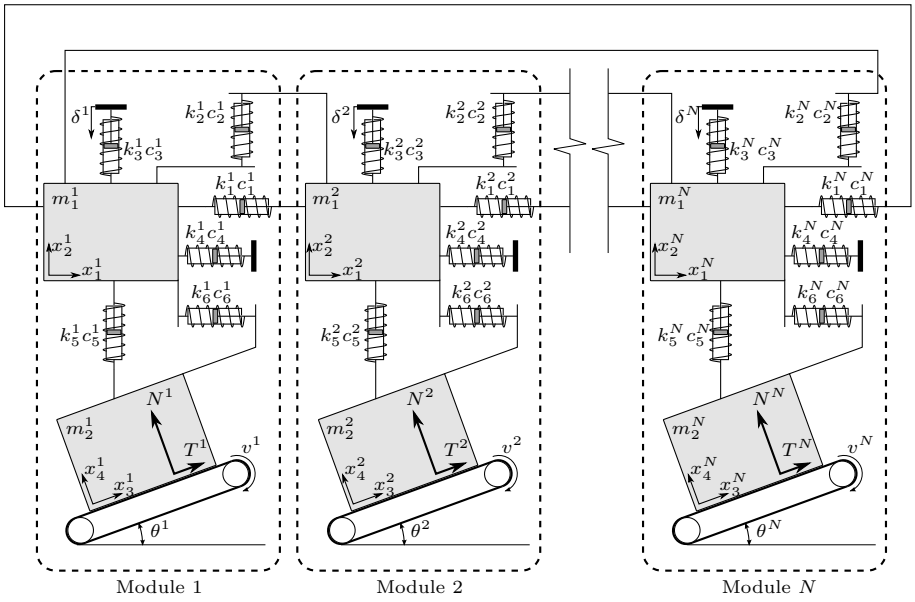

Figure 1: Periodic and N-modular lumped system

Before the application of the contact constraint, in a general configuration, each module is characterized by 4 Degrees of Freedom (DoF):

$$\boldsymbol{X}^i = \left\{ \begin{array}{cccc} x_1^i & x_2^i & x_3^i & x_4^i \end{array} \right\}^T. \tag{1}$$

The mass sub-matrix of the single module is

$$\mathbf{M}^i = \mathrm{diag}(\begin{array}{cccc} m_1^i & m_1^i & m_2^i & m_2^i \end{array}) \tag{2}$$

The stiffness sub-matrix of the single module is:

$$\mathbf{K}^i = \left[\begin{array}{cccc|cc} k_1^i + k_4^i + k_6^i & 0 & -k_6^i \cos\theta^i & k_6^i \sin\theta^i & -k_1^i & 0 \\ 0 & k_2^i + k_3^i + k_5^i & -k_5^i \sin\theta^i & -k_5^i \cos\theta^i & 0 & -k_2^i \\ -k_6^i \cos\theta^i & -k_5^i \sin\theta^i & k_5^i \sin^2\theta^i + k_6^i \cos^2\theta^i & (k_5^i - k_6^i) \sin\theta^i \cos\theta^i & 0 & 0 \\ k_6^i \sin\theta^i & -k_5^i \cos\theta^i & (k_5^i - k_6^i) \sin\theta^i \cos\theta^i & k_5^i \cos^2\theta^i + k_6^i \sin^2\theta^i & 0 & 0 \\ \hline -k_1^i & 0 & 0 & 0 & k_1^i & 0 \\ 0 & -k_2^i & 0 & 0 & 0 & k_2^i \end{array} \right] \tag{3}$$

the elements of this matrix over the 4^{th} line and column represent the link between the module i and the module $i+1$. To realize the periodicity condition the N^{th} module is linked with the 1^{st} module. These sub-matrices, defined for each module, are assembled to obtain the full matrices $\mathbf{M}$ and $\mathbf{K}$ $(4N \times 4N)$ of the mechanical system. The material damping is considered to be proportional to the mass and to the stiffness of the system, following the Rayleigh model, and the damping matrix can be defined as follows:

$$\mathbf{C} = \alpha\mathbf{M} + \beta\mathbf{K}. \tag{4}$$

The vector of the applied forces for the i^{th} module is:

$$\boldsymbol{F}^i = \left\{ \begin{array}{cccc} 0 & -k_3^i \delta^i & T^i & N^i \end{array} \right\}^T \tag{5}$$

Hence, the dynamic equation of motion can be written for the mechanical system:

$$\mathbf{M}\ddot{\boldsymbol{X}} + \mathbf{C}\dot{\boldsymbol{X}} + \mathbf{K}\boldsymbol{X} = \boldsymbol{F} \tag{6}$$

The contact conditions

$$\begin{cases} x_4^i N^i = 0 \\ x_4^i \geq 0 \quad \text{and} \quad N^i \geq 0 \\ T^i = -\text{sign}(\dot{x}_3^i - v^i)\mu N^i \end{cases} \tag{7}$$

impose some constraints on the system, reducing the actual number of DoFs of each module. The contact between the mass m_2^i and the respective slider of each module i can assume 4 different states:

Sliding (SL): in this state the tangential speed of the contacting mass is lower than the slider speed ($\dot{x}_3^i < v^i$); the tangential force can be expressed as a function of the normal force by means of the friction coefficient μ ($T^i = \mu N^i$). Furthermore, the contact condition imposes that the position, velocity and acceleration in the direction x_4^i, that are normal to the contact, are nil ($x_4^i = \dot{x}_4^i = \ddot{x}_4^i = 0$). In these conditions the local normal force, acting on the contact mass, is calculated as a function of the system state ($N^i = f(\boldsymbol{X}, \dot{\boldsymbol{X}})$);

Reverse-sliding (R-SL): in this state the tangential speed of the contacting mass is higher than the slider speed ($\dot{x}_3^i > v^i$). Concerning the direction normal to the contact, the same considerations for the SL state remains valid; nevertheless, in this case, the tangential force has an opposite direction ($T^i = -\mu N^i$);

Sticking (ST): in this state the relative speed between the contacting mass and the slider is nil ($\dot{x}_3^i = v^i$). Also in this case the mass m_2^i does not move in the direction normal to the contact and both the normal and tangential forces can be expressed as a function of the system state $N^i = f_1(\boldsymbol{X}, \dot{\boldsymbol{X}})$ and $T^i = f_2(\boldsymbol{X}, \dot{\boldsymbol{X}})$. To remain in ST state the module of the tangential force must be $|T^i| < \mu N^i$. When $|T^i|$ reaches the limit value μN^i the system switch to the SL or R-SL state, as a function of the sign of the tangential force T^i;

Detachment (DT): when the normal force N^i reaches a nil value, the unilateral contact constraint cannot apply a traction force on the mass ($N^i \geq 0$) and the mass detaches from the slider moving in both the normal ($x_4^i \geq 0$) and tangential direction. In this case the contact forces are nil ($N^i = T^i = 0$) until the normal position $x_4^i > 0$. When the normal position reaches the nil value it means that the mass engages again the contact with the slider and the system switches to the SL or R-SL state, as a function of the sign of the relative tangential speed.

When at least one of the modules composing the system is in SL or R-SL state, the tangential force has the following form:

$$T^i = -\text{sign}(x_3^i - v^i)\mu f\left(\boldsymbol{X}, \dot{\boldsymbol{X}}\right) \tag{8}$$

and introduces asymmetric terms on the stiffness and damping matrices.

Furthermore, when at least one of the contacting masses is in ST state, with the slider that moves with a constant speed v^i, the position of the sticking mass is:

$$x_3^i(t) = \hat{x}^i + v^i(t - \hat{t}) \tag{9}$$

where $\hat{x}^i$ and $\hat{t}$ are respectively the tangential position of the sticking mass at the beginning of the ST state and the time at beginning of the ST state.

Hence, after the application of the contact constraints, in (8) and (9), the dynamic equation of the system, in (10), will be characterized by system matrices $\widetilde{\mathbf{M}}$, $\widetilde{\mathbf{C}}$ and $\widetilde{\mathbf{K}}$ that are generally smaller than the matrices in (6) and they will be non-symmetric if at least one of the contacting masses is in SL or R-SL state. Furthermore, the applied forces on the right side of (10) will be composed by constant terms $\boldsymbol{F_0}$ if all the masses are in SL, R-SL or DT state. A time dependent linear terms $\boldsymbol{F_1}t$ will appear if at least one of the contacting mass is in ST state. A general system of equation can be expressed as:

$$\widetilde{\mathbf{M}}\ddot{\widetilde{\boldsymbol{X}}} + \widetilde{\mathbf{C}}\dot{\widetilde{\boldsymbol{X}}} + \widetilde{\mathbf{K}}\widetilde{\boldsymbol{X}} = \boldsymbol{F_0} + \boldsymbol{F_1}t \tag{10}$$

2.2. Time integration approach

The defined mechanical system (cf. Fig. 1), due to its lumped nature, can reach a finite number of contact configurations (4^N). During the transient response, the system remains into the same contact configuration for a finite interval of time. The dynamic equations (10) can be assembled and calculated for each contact configuration and an analytical solution can be obtained. During each interval, the response of the system can be expressed with a modal decomposition approach [32]. The asymmetry of the stiffness and damping matrices forces us to write the mechanical equation in the state space coordinates $\boldsymbol{Y}$ as follows:

$$\begin{cases} \widetilde{\mathbf{M}}\ddot{\widetilde{\boldsymbol{X}}} + \widetilde{\mathbf{C}}\dot{\widetilde{\boldsymbol{X}}} + \widetilde{\mathbf{K}}\widetilde{\boldsymbol{X}} = \boldsymbol{F_0} + \boldsymbol{F_1}t \\ \widetilde{\mathbf{M}}\dot{\widetilde{\boldsymbol{X}}} - \widetilde{\mathbf{M}}\dot{\widetilde{\boldsymbol{X}}} = \mathbf{0} \end{cases} \tag{11}$$

$$\mathbf{A} = \begin{bmatrix} \widetilde{\mathbf{C}} & \widetilde{\mathbf{M}} \\ \widetilde{\mathbf{M}} & \mathbf{0} \end{bmatrix}, \ \mathbf{B} = \begin{bmatrix} \widetilde{\mathbf{K}} & \mathbf{0} \\ \mathbf{0} & -\widetilde{\mathbf{M}} \end{bmatrix}, \tag{12}$$

$$\boldsymbol{Y} = \begin{Bmatrix} \widetilde{\boldsymbol{X}} \\ \dot{\widetilde{\boldsymbol{X}}} \end{Bmatrix}, \ \boldsymbol{Q_0} = \begin{Bmatrix} \boldsymbol{F_0} \\ \mathbf{0} \end{Bmatrix} \text{and } \boldsymbol{Q_1} = \begin{Bmatrix} \boldsymbol{F_1} \\ \mathbf{0} \end{Bmatrix} \tag{13}$$

$$\mathbf{A}\dot{\boldsymbol{Y}} + \mathbf{B}\boldsymbol{Y} = \boldsymbol{Q_0} + \boldsymbol{Q_1}t. \tag{14}$$

To perform the Complex Eigenvalue Analysis (CEA), two eigenproblems have to be defined on (14), to find the complex eigenvalues λ and both the left and right complex eigenvectors, respectively $\boldsymbol{\upsilon}$ and $\boldsymbol{\xi}$, as follows:

$$\lambda_r \boldsymbol{\upsilon_r}^T \mathbf{A} = -\boldsymbol{\upsilon_r}^T \mathbf{B} \tag{15}$$

$$\lambda_r \mathbf{A}\boldsymbol{\xi_r} = -\mathbf{B}\boldsymbol{\xi_r} \tag{16}$$

Left and right complex eigenvectors can be gathered on matrices, respectively $\boldsymbol{\Upsilon}$ and $\boldsymbol{\Xi}$ that allows to diagonalize the system matrices $\mathbf{A}$ and $\mathbf{B}$ in (14):

$$\boldsymbol{\Upsilon}^T \mathbf{A} \boldsymbol{\Xi}\, \dot{\boldsymbol{z}} + \boldsymbol{\Upsilon}^T \mathbf{B} \boldsymbol{\Xi}\, \boldsymbol{z} = \boldsymbol{\Upsilon}^T \boldsymbol{Q_0} + \boldsymbol{\Upsilon}^T \boldsymbol{Q_1} t \tag{17}$$

$$\begin{bmatrix} \ddots & \\ & a_r \\ & & \ddots \end{bmatrix} \dot{\boldsymbol{z}} + \begin{bmatrix} \ddots & \\ & b_r \\ & & \ddots \end{bmatrix} \boldsymbol{z} = \boldsymbol{p_0} + \boldsymbol{p_1} t. \tag{18}$$

where $\boldsymbol{z}$ is the vector of the complex modal coordinates. The right eigenvector matrix $\boldsymbol{\Xi}$ allows the transformation between the state space coordinates and the modal coordinates $\boldsymbol{Y} = \boldsymbol{\Xi}\boldsymbol{z}$; $\boldsymbol{p_0}$ and $\boldsymbol{p_1}$ are the projection on the modal base, by means of the left eigenvector matrix $\boldsymbol{\Upsilon}$, of the constant and of the linear term of the applied forces $\boldsymbol{Q_0}$ and $\boldsymbol{Q_1}$. Furthermore, a_r and b_r represent the diagonal terms after the modal transformation.

Finally, the response of the system, starting from the initial condition $\boldsymbol{Y_0}$, can be expressed as:

$$\boldsymbol{Y}(t) = \boldsymbol{\Xi} \begin{bmatrix} \ddots & \\ & e^{\lambda_r t} \\ & & \ddots \end{bmatrix} \boldsymbol{\Xi}^{-1} \boldsymbol{Y_0} + \boldsymbol{\Xi} \begin{bmatrix} \ddots & \\ & b_r \\ & & \ddots \end{bmatrix}^{-1} \begin{bmatrix} \ddots & \\ & 1 - e^{\lambda_r t} \\ & & \ddots \end{bmatrix} \boldsymbol{p_0} + \boldsymbol{\Xi} \begin{bmatrix} \ddots & \\ & b_r \\ & & \ddots \end{bmatrix}^{-1} \begin{bmatrix} \ddots & \\ & \dfrac{1 - e^{\lambda_r t}}{\lambda_r} + t \\ & & \ddots \end{bmatrix} \boldsymbol{p_1} \tag{19}$$

The solution in (19) is valid within a time interval, until one of the contact masses changes its contact state at time $t^\star$. The position and velocity of the system at this time $\boldsymbol{Y}(t^\star)$ will be the initial condition $\boldsymbol{Y_0}$ for the following time interval; the time response within the new time interval is still expressed by (19), but calculated starting from a set of system dynamic equations in (10) that account for the new contact configuration of the system. In such a way, the time response of the system is piecewise linear and can be calculated in subsequent time intervals by considering the set of dynamic equations appropriate to each contact configuration of the system.

2.3. Definition of the energy quantities

The transient simulation is performed starting with the system at its static equilibrium position $\boldsymbol{X_0}$, due to the application of the static pre-load δ^i, while the sliders are driven at a constant velocity v during the

whole simulation. A small perturbation ε from the equilibrium is applied to one of the degrees of freedom, in the state space, in order to observe the transient response and the stability of the frictional system [32].

The transient simulation allows for calculating the response $\boldsymbol{Y}(t)$ at each time interval, taking into account the contact state variation during the system response.

The mechanical energy E_t of the system can be expressed as sum of the kinetic E_k and elastic potential E_e energies. They can be calculated from the transient solutions $\boldsymbol{X}(t)$ and $\dot{\boldsymbol{X}}(t)$

$$E_k(t) = \frac{1}{2}\dot{\boldsymbol{X}}(t)^T \mathbf{M}\dot{\boldsymbol{X}}(t) \tag{20}$$

$$E_e(t) = \frac{1}{2}\boldsymbol{X}(t)^T \mathbf{K}\boldsymbol{X}(t). \tag{21}$$

To calculate the potential term, only the elastic force have to be considered; consequently, to compute this quantity the matrix $\mathbf{K}$ in (6) has to be considered, rather than the matrix $\widetilde{\mathbf{K}}$ in (10), which includes also the non-conservative terms due to the contact forces.

Based on the work-energy theorem, the work of non-conservative forces produces a variation of the mechanical energy. In this system the two non-conservative forces are the tangential contact forces T^i and the internal damping forces F_d:

$$\boldsymbol{F_d}(t) = \mathbf{C}\dot{\boldsymbol{X}}(t) \tag{22}$$

The material dissipated power $P_m(t)$ and the power $P_c(t)$ exchanged at the contact can be expressed as follows:

$$P_m(t) = \dot{\boldsymbol{X}}(t)^T \mathbf{C}\dot{\boldsymbol{X}}(t) \tag{23}$$

$$P_c(t) = \sum_{i=1}^{N} T^i(t)\, \dot{x}_3^i(t). \tag{24}$$

The sign of the contact exchanged power P_c indicates the direction of the energy flow at the contact and, for each term, it depends on the direction of the tangential speed $\dot{x}_3^i$ and of the tangential contact force T^i. Each contacting mass m_2^i gives its positive or negative contribution over the simulation time.

Hence, the derivative of the total energy can be expressed as the sum of the power exchanged at the contact and the power dissipated by the damping forces [33]:

$$\frac{dE_t(t)}{dt} = P_c(t) - P_m(t) \tag{25}$$

The damping dissipative term P_m gives always a negative contribution to the variation of the mechanical energy E_t, due to the nature of the damping non-conservative forces that produce an action proportional to the velocity along the opposite direction with respect to the local velocity. On the other hand the power exchanged at the contact P_c between the elastic system and the sliders can be either positive, increasing the energy content of the system E_t, or negative, subtracting energy from the system and acting as a damper with respect to the dynamic response of the system. In general, during friction-induced vibrations, a mutual exchange in the two directions is always present at the contact.

It should be noted that P_c is the energy exchanged and not the energy dissipated at the contact, even if it has a negative sign. In fact, a distinction must be done between the exchanged energy at the contact P_c and the energy dissipated at the contact P_d, which is defined as the product of the relative velocity $(x_3^i - v^i)$ and the tangential component of the contact force T^i:

$$P_d(t) = \sum_{i=1}^{N} (\dot{x}_3^i - v^i) T^i \tag{26}$$

This quantity is always negative both in SL and in R-SL state, because of the definition of the tangential force in (8). The masses in ST state have a nil relative velocity and their contribution to the contact dissipated power is zero.

Finally, the total external power P_{ex}, released by the sliders, is defined as

$$P_{ex} = \sum_{i=1}^{N} v^i T^i \tag{27}$$

and it is partially dissipated at the contact P_d and partially introduced into the elastic system P_c (28).

$$P_{ex} = P_d + P_c. \tag{28}$$

3. System response and energy analysis

In this section, results by the transient analysis and CEA are presented to show the capability of this system to reproduce friction-induced vibrations in unstable conditions. Moreover, the time evolution of the system energy analysis terms, detailed in the paragraph 2.3, is analyzed.

The transient responses are presented for a system composed by two modules ($N = 2$ in Fig. 1), where the masses m, the springs stiffness k, the inclination angle θ, the pre-load δ and the damping coefficients α and β in (4) are reported in Table 1.

Parameter	**Value**	**Unity**
$m^i_{1:2}$	{ 0.3 0.7 }	kg
$k^i_{1:6}$	{ 5.5 6.0 2.2 6.0 30.0 25.0 }E + 4	N/m
θ^i	0.5	rad
δ^i	5.0E − 3	m
α	0.0	s^{-1}
β	3.0E − 5	s

Table 1: System parameters and boundary conditions.

The physical (masses, stiffness and damping of the lumped model) and the geometrical parameters (plane inclination angles), which have been adopted for these analyses, have been arbitrarily chosen in order to obtain a system with multiple instabilities.

Figure 2(a) shows the values of real and imaginary parts of the eigenvalues λ obtained by CEA and their dependence on the friction coefficient μ. Figure 2(b) shows the real mode shapes for a nil friction coefficient.

The friction coefficient μ, as well as the damping coefficients α and β, are considered to be key factors in the system stability [17, 29, 30, 34] because the two terms in (25) are strictly related to them.

Increasing the friction coefficient μ for the same value of all the other system parameters, the weight of the contact term P_c, in the energy balance (25), and of the energy that is actually dissipated at the contact P_d (26) increases.

From a mathematical point of view, the asymmetric contribution in $\widetilde{\mathbf{K}}$ and $\widetilde{\mathbf{C}}$ (10) due to the frictional contact interaction in SL or R-SL state (8), grows as a function of μ. This modifies the eigenvalues and eigenvectors of the system in (15) and (16); if the frequencies of two similar modes coalesce, it produces the lock-in phenomena with a consequent divergence of the real parts of the coalesced eigenvalues (cf. Fig. 2(a)). The system becomes unstable if one of the real parts reaches a positive value. In the parametric analysis in Fig. 2(a), the range of variation of the friction coefficient μ has been selected in order to obtain several unstable modes, with the real parts of the unstable eigenvalues that cross each other as μ increases.

It is worth noting that the coalesced modes (cf. Fig. 2) are characterized by a displacement of the upper masses that is in phase one each other for modes $3 - 4$, and in phase opposition for modes $5 - 6$; the same observation can be done for the contact masses. Furthermore, observing each pair of coalesced modes, one of the two modes is characterized by displacements of the upper masses that are quasi-normal to the slider, while the other is quasi-parallel. When the modes coalesce to each other, the combination of these displacement directions (normal and tangential to the contact surface) generates a quasi-elliptic motion of the upper masses that is at the origin of the energy exchange between the mechanical system and the contact, i.e. of the stability or instability of the system [32]. This quasi-elliptic motion is, in fact, at

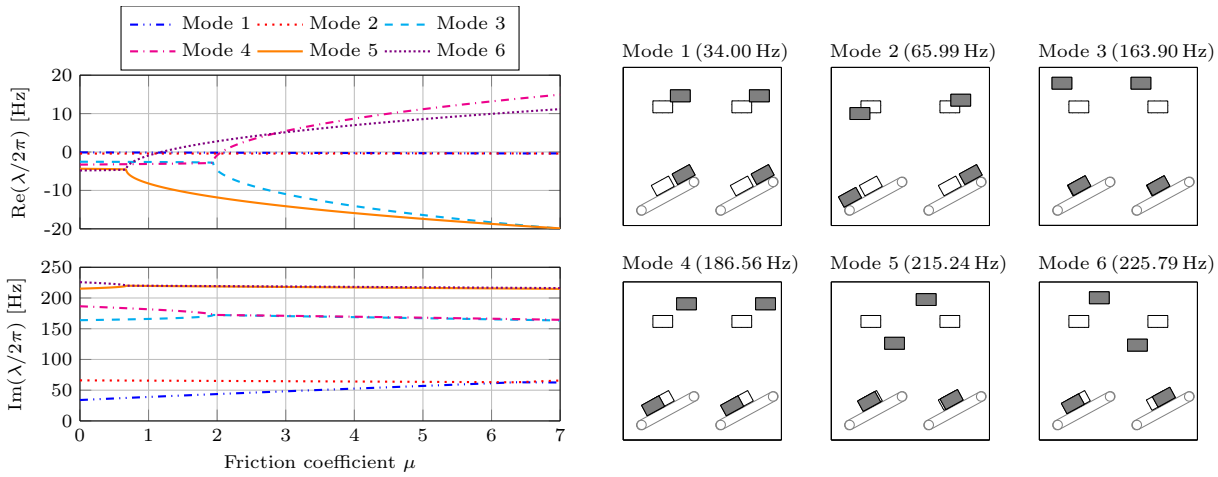

(a) Real and Imaginary part of the complex eigenvalue λ as function of the friction coefficient μ

(b) Real mode shapes for $\mu = 0$

Figure 2: Complex Eigenvalues Analysis results and stability evaluation.

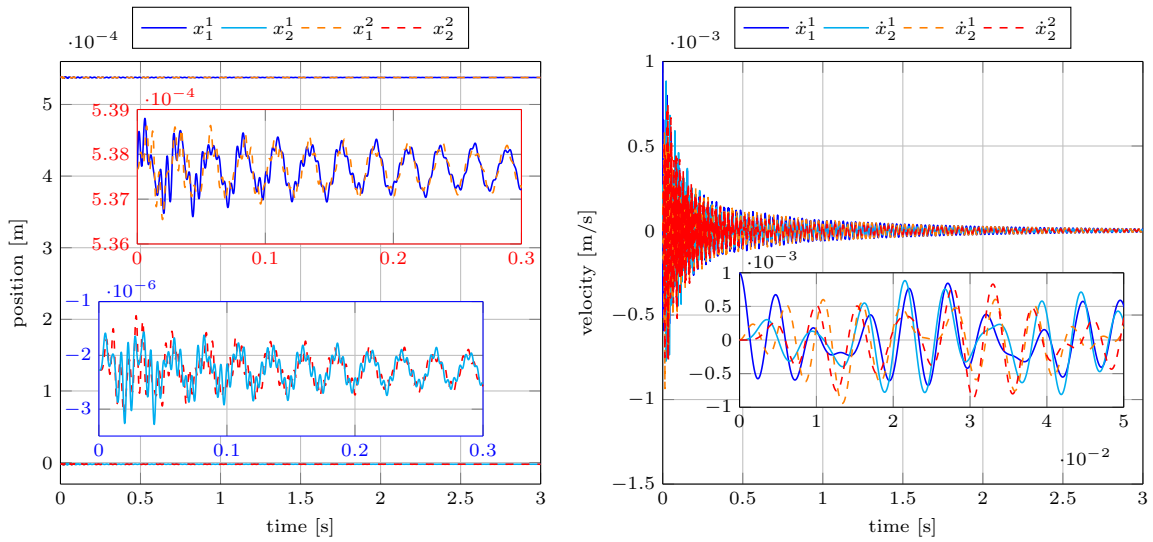

(a) Position response of masses m_1^i.

(b) Velocity response of masses m_2^i.

Figure 3: Stable response of the system composed by two modules $N = 2$ for a friction coefficient $\mu = 1$

the origin of the phase difference between the tangential speed and the tangential force that produces the contact energy flow [18, 19, 32].

On the contrary, the modes 1 and 2 are characterized by a quasi rigid motion of the modules along the direction of the sliders. Their deformation does not produce any variation of the normal contact force N; this is the reason why the two modes, even if they reach the same frequency, for a friction coefficient $\mu \simeq 6.5$, don't coalesce and pass through each other (in frequency) without interacting. The presence of tangential and normal components of the coalescing modes at the contact interface has been found to be a necessary requirement for mode instability in finite element models of continuous systems and experiments [35, 36].

3.1. Stable transient behavior

The study of the eigenvalue real parts is a standard tool to investigate the system stability. When all the eigenvalue real parts are negative, the system is stable and the transient response converges exponentially to the static equilibrium position. On the contrary, when at least one of the eigenvalue has a positive real part, the system is unstable and the response diverges.

Using this criterion, the system introduced in Section 3 is stable for a friction coefficient $\mu < 1.19$ (cf. Fig. 2(a)). In particular, for the friction coefficient $\mu = 1$, even if modes $5-6$ are already coalesced, all the real parts are still negative. The system response is reported in Fig. 3. In this case the initial condition is the static equilibrium position $\boldsymbol{X_0}$ due to the application of the static pre-load $\delta^{1:2}$ (cf. Fig. 3(a)) with a perturbation applied on the velocity $\dot{x}_1^1(0) = \varepsilon = 0.001$m/s (cf. Fig. 3(b)).

3.2. Unstable transient behavior

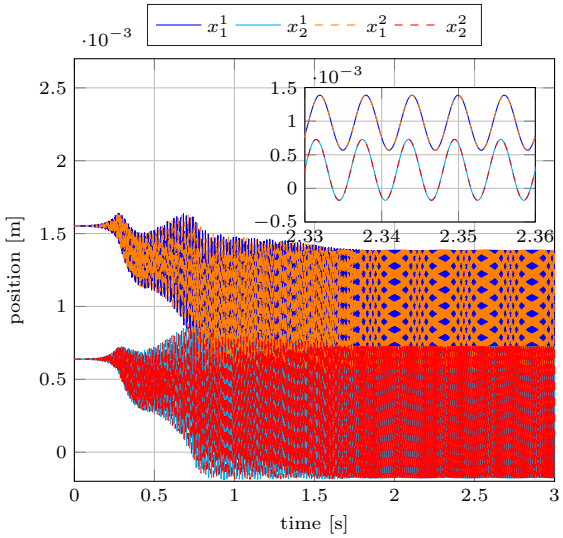

(a) Position response of masses m_1^i.

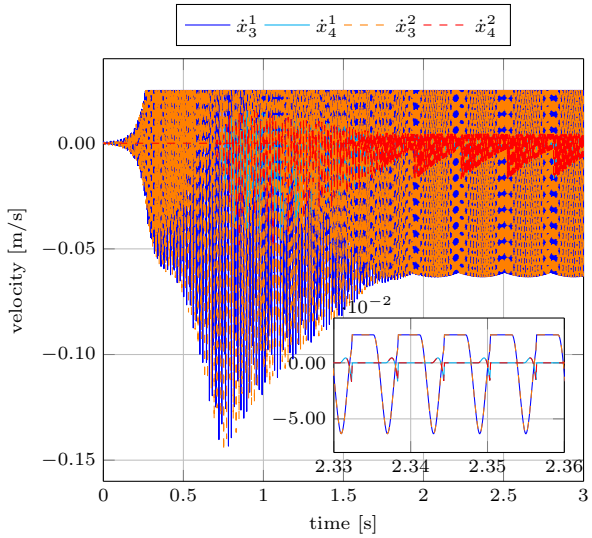

(b) Velocity response of masses m_2^i.

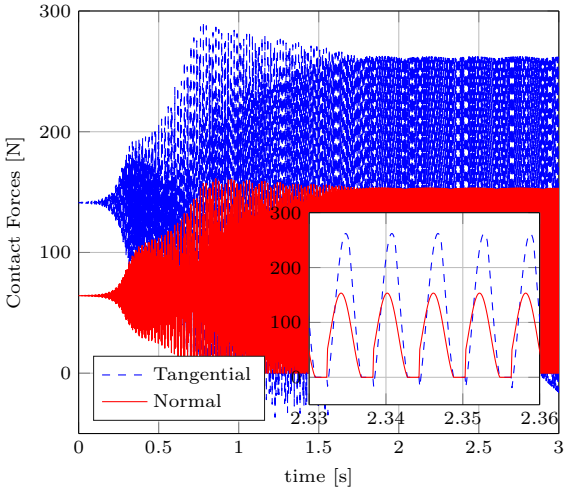

(c) Contact forces on mass m_2^1

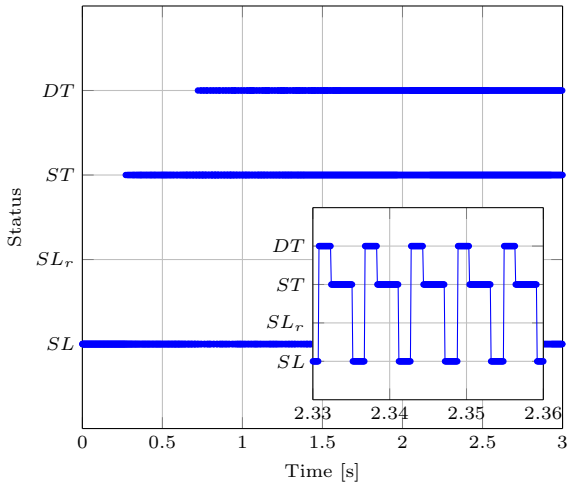

(d) Contact status on mass m_2^1

Figure 4: Unstable response of a system composed by two modules $N = 2$ for a friction coefficient $\mu = 2.2$

For the same model, in case of a friction coefficient $\mu = 2.2$ the system is unstable, the coalesced modes $3-4$ and $5-6$ have a positive real part (cf. Fig. 2(a)), and the same small perturbation ε (as in Section 3.1) generates a transient response with an amplitude that increases exponentially (cf.Fig. 4).

Figure 4 shows the transient response of the system, when self-excited friction-induced vibrations arise. The amplitude of vibration increases with a complex behavior due to the presence of more than one unstable mode ($t < 1.5s$ in Fig. 4(a)). After an initial phase of increasing amplitude (in overall sliding condition) ($t < 0.4s$), an intermediate saturation phase occurs, where the contact nonlinearities (switch between different contact state) heavily modify the linear behavior ($0.5 < t < 1.5s$); afterwards the system reaches a steady-state behavior ($t > 2s$), characterized by the limit-cycle.

The steady-state transient response is periodic (limit-cycle) and the two subsystems are in phase with each other (cf. magnified responses in Fig. 4(a) and Fig. 4(b)). During this steady state behavior the two contact masses switch between SL, ST (when the $\dot{x}_3^i = v^i = 2.5m/s$ in Fig. 4(b)) and DT (when $\dot{x}_4^i \neq 0$ in Fig. 4(b)). Figures 4(c) and 4(d) show respectively the contact force and the contact status of the mass m_2^1 to give a better idea of the relevance of the contact nonlinearities in the transient behavior (i.e. stick-slip transition in the tangential direction, and contact-no contact transitions in the normal direction).

When the system reaches a steady state condition, the global amplitude of vibration remains constant, i.e. the integral of the power exchanged over a period of oscillation (25) is nil.

3.3. Weakness of the eigenvalue real part as unstable mode selector

It is known that the main drawback of CEA is the over-prediction of the instabilities [5, 15, 17, 35]. CEA parametric analysis gives as a result all the possible unstable system modes, with over-prediction of the unstable ranges and with the impossibility to predict which mode will be effectively unstable, when several modes are predicted to have a positive real part of the eigenvalue. A higher value of a real part does not correspond to the probability of the mode to become unstable in the transient response, but only to the rate of growth of the vibrations in the initial linear phase before the nonlinear contact transitions. The previous simulations in Section 3.1 and Section 3.2 show the reliability of the real part of the system eigenvalues to evaluate the stability of the system; on the contrary it is not possible, by observation of the real parts, to identify the "effectively unstable" mode in the case of system multi-instabilities (i.e. when more than one eigenvalues of the system have a positive real part) and to indicate the modal instability that would be recovered on the steady state transient response. For example in the unstable response presented in Section 3.2 the modes $3-4$ and $5-6$ are in a lock-in state, their real parts (respectively $\mathrm{Re}(\lambda_{3-4}) = 1.292\mathrm{Hz}$ and $\mathrm{Re}(\lambda_{5-6}) = 3.317\mathrm{Hz}$) are positive and the system is unstable. During the initial part of the transient response ($t < 0.25\mathrm{s}$), when the system is in a uniform sliding state (cf. Fig. 4(b)), the frequency analysis in Fig. 5(b) shows the presence of the two unstable modes with an amplitude of their frequency peak that depends on both the real part and the particular perturbation chosen for this analysis. The resulting contact nonlinearities ($0.5\mathrm{s} < t < 1.5\mathrm{s}$) produces the increase of the contribution of modes $3-4$ on the system response. Finally, the frequency analysis of the unstable transient response in the time interval $2\mathrm{s} < t < 3\mathrm{s}$ shows a single peak in the spectrum (with some small super-harmonic contributions) corresponding to the frequency $f \simeq 166\mathrm{Hz}$ of the coalesced mode $3-4$, which is the one with the lower value of the real part.

Furthermore, an analysis of the transient responses (cf. Fig. 4) shows that the two modules move perfectly in phase one each other, confirming the same deformation of the corresponding $3-4$ coalesced real modes (cf. Fig. 2(b)), which is characterized by the same motion of the two subsystems.

4. A new instability index for mode selection based on energy considerations

As highlighted in 3.3, the real part of the unstable eigenvalue is not able to predict the real propensity of each unstable mode to squeal. In this section a new index is defined, based on the observation that the unstable modes are the ones with a more relevant deformation at the contact [17], which increases the energy flow at the contact. The idea is to compute, for each mode, the variation of the total energy E_t due to the power P_c introduced by the contact during friction induced vibrations and the power P_m dissipated by

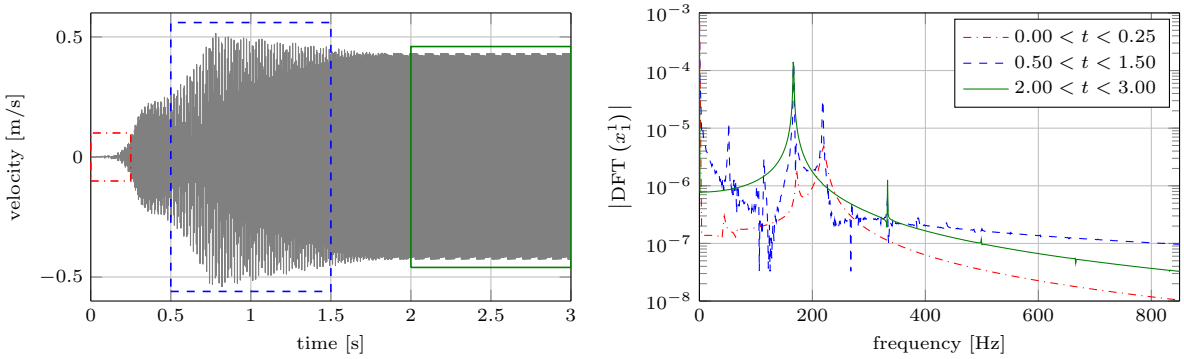

(a) Velocity response along x_1^1

(b) Discrete Fourier Transform

Figure 5: Frequency analysis of the unstable transient response of a $N = 2$ system with a friction coefficient $\mu = 2.2$.

material damping, evaluated as mean values over an oscillation period for each eigenvector of the system. In this way, it is possible to have a comparison between different modes, not only based on the information coming from the eigenvalues (eigenfrequencies and modal dampings) but also on the eigenvectors (modal shapes), which contain important information about the energy distribution over the system, and on the capability of each mode to absorb and dissipate energy from both the contact and the bulk.

The distribution of stresses in combination with the local tangential velocity at the contact interface are related to the capability of each mode to introduce energy into the system. These considerations can be made by referring to each complex eigenvector (complex modal shape) resulting from the CEA; nevertheless, each mode contribution is defined as proportional to an arbitrary constant that is complex and generally different for left and right modes in case of non self-adjoint systems (cf. (15) and (16)).

To account for the contribution of each mode, a decomposition on the modal base, by means of the left and right eigenvectors ($\boldsymbol{\Upsilon}$ and $\boldsymbol{\Xi}$), of the static equilibrium position $\widetilde{\boldsymbol{X_0}}$ is proposed here. In this manner also the contact forces in the static equilibrium position (overall sliding) are projected over the modal base. In fact, the static equilibrium position is the actual deformation of the system in the steady-state condition (braking phase) without instabilities induced by the contact; the friction-induced vibrations produce an oscillation of the system around this position. During the sliding contact, the contact interaction produces a large band excitation on the mechanical system, which is spatially distributed as the contact forces. In this analysis the contact forces are evaluated at the static equilibrium position in uniform sliding, since it represents the spatial distribution of the starting boundary condition for the unstable vibrations. Hence, the contribution of such excitation to each system mode is proportional to the modal projection of the static equilibrium position on the complex modal base. In this way, the projection of the equilibrium position on the system modes allows for comparing the energy amount absorbed by each mode during the vibrations around the equilibrium position (steady-state deformation), that are generated by a wide-band perturbation with the same geometrical distribution as the static contact force. The static solution

$$\widetilde{\mathbf{K}}\widetilde{\boldsymbol{X_0}} = \boldsymbol{F_0} \tag{29}$$

can be expressed in the state space coordinate

$$\mathbf{B}\boldsymbol{Y_0} = \boldsymbol{Q_0} \tag{30}$$

where $\mathbf{B}$ is the system matrix in the state coordinates defined in (12) and $\boldsymbol{Y_0}$ and $\boldsymbol{Q_0}$ are respectively the static equilibrium state of the system and the corresponding external forces defined in the state coordinates (cf. (13)). The matrix $\mathbf{B}$ in (30) can be diagonalized by means of the system eigenvectors matrices (cf. (18)):

$$\boldsymbol{\Upsilon}^T\mathbf{B}\boldsymbol{\Xi}\boldsymbol{z_0} = \begin{bmatrix} \ddots & & \\ & b_r & \\ & & \ddots \end{bmatrix}\boldsymbol{z_0} = \boldsymbol{\Upsilon}^T\boldsymbol{Q_0} \tag{31}$$

where b_r represents the r^{th} element of the diagonal matrix.

The complex eigenvalues are complex and conjugate ($\lambda_r^\star = \lambda_{r+1}$ where * indicates the complex and conjugate operation); the elements on the even columns of the complex eigenvectors matrices are the complex and conjugate of the previous odd columns ($\boldsymbol{\upsilon_r^\star = \upsilon_{r+1}}$ and $\boldsymbol{\xi_r^\star = \xi_{r+1}}$). Hence, the modal contributions $\boldsymbol{z_0}$ are 2×2 complex and conjugates ($z_r^\star = z_{r+1}$) and the sum of a couple of these gives a real contribution on the state space. Finally, it is possible to consider the contribution on the system position of each complex and conjugate couple of modes as follows:

$$\boldsymbol{Y_r} = \frac{1}{b_r}\boldsymbol{\xi_r \upsilon_r^T Q_0} \tag{32}$$

$$\boldsymbol{Y_{r+1}} = \boldsymbol{Y_r^\star} = \frac{1}{b_{r+1}}\boldsymbol{\xi_{r+1} \upsilon_{r+1}^T Q_0} \tag{33}$$

and being these contributions complex and conjugates their sum is real too.

Quantities in (32) and (33) contain information about both the position $\widetilde{\boldsymbol{X_r}}$ and the velocity $\dot{\widetilde{\boldsymbol{X}}}_{\boldsymbol{r}}$ for each couple of complex and conjugated modes; hence, the corresponding contact forces $\boldsymbol{N_r}$ and $\boldsymbol{T_r}$ can be calculated.

The damping forces $\boldsymbol{F_d}$ are expressed as the product of the damping matrix $\widetilde{\mathbf{C}}$ times the speed vector $\dot{\widetilde{\boldsymbol{X}}}$; it is possible as well to calculate the damping forces $\boldsymbol{F_{d,r}}$ generated by each modal contribution $\dot{\widetilde{\boldsymbol{X}}}_{\boldsymbol{r}}$.

$$\boldsymbol{F_{d,r}} = \widetilde{\mathbf{C}}\dot{\widetilde{\boldsymbol{X}}}_{\boldsymbol{r}} \tag{34}$$

The modal contribution of the system speed $\dot{\widetilde{\boldsymbol{X}}}_{\boldsymbol{r}}$ and the modal contribution of the damping forces $\boldsymbol{F_{d,r}}$, are complex quantities, and for both of them it is possible to define a modulus (indicated respectively by $\boldsymbol{\Lambda_r}$ and $\boldsymbol{\Gamma_r}$) and phase (indicated respectively by $\boldsymbol{\Phi_r}$ and $\boldsymbol{\Psi_r}$). The mean power dissipated by material damping for each mode during a period of oscillation is:

$$\widehat{P}_{m,r} = 2\boldsymbol{\Lambda_r^T}\left[\boldsymbol{\Gamma_r} \odot \cos\left(\boldsymbol{\Phi_r - \Psi_r}\right)\right] \tag{35}$$

where $\odot$ indicates the Hadamard product (element by element product) of the two vectors.

The mean power introduced into the system by the frictional contact $\widehat{P}_{c,r}$ can be expressed, for each mode, during a period of oscillation, as the sum of the power exchanged by each contact mass. Each contribution can be expressed as the product of the modulus τ_r^i of tangential force T_r^i and the modulus ρ_r^i of the tangential speed $\dot{x}_{3,r}^i$, times the cosines of the difference of phases, respectively ψ_r^i and ϕ_r^i:

$$\widehat{P}_{c,r} = 2\sum_{i=1}^{N} \tau_r^i \rho_r^i \cos\left(\psi_r^i - \phi_r^i\right). \tag{36}$$

The Modal Absorption Index (MAI) is defined as the ratio between the total energy variation $\Delta E_{t,r}$, over a period of oscillation Δt_r, and the period of oscillation itself. It is given by the sum of the mean contribution of the Contact exchanged Power and the Material Dissipated Power for each couple of complex and conjugate modes:

$$\chi_r = \frac{\Delta E_{t,r}}{\Delta t_r} = \widehat{P}_{c,r} + \widehat{P}_{c,r+1} - \widehat{P}_{m,r} - \widehat{P}_{m,r+1}. \tag{37}$$

The MAI allows for comparison of the different system modes, by describing their respective capability to absorb energy by the environment and to generate squeal. The information coming from this quantity results to be particularly interesting in case of systems characterized by multi-instabilities highlighted by CEA, where the standard approach does not give further information about the effective steady-state behavior.

The use of the static position decomposition allows to take into account the "shape" of the excitation at the contact zone. In the numerical model, during the first part of the response, in uniform sliding condition, the energy is introduced into the system at the contact interface by the frictional forces; the

contribution of each mode on the transient behavior is strictly related to the initial external perturbation and to the modal damping factor (real part of the corresponding eigenvalue). During the relative motion, the random excitation from the sliding surface and the local variations of contact state (local sticking and/or detachment) generate a uniform wide-band excitation that involves all the system modes; the mode with a higher capability to introduce energy into the mechanical system is the one that will mainly affect the steady-state response.

5. Application of the instability index to the lumped model

5.1. Application to the 2-modules system

Using the quantities introduced in Section 4 for the model analyzed in Section 3, it is possible to highlight that the MAI, in combination with the information provided by the complex eigenvalues, is able to predict the transient behavior of the unstable system. Several transient analyses have been performed to highlight the different behaviors of the unstable system for several values of the friction coefficient (cf. Fig. 2).

Table 2 shows the 12 complex and conjugated eigenvalues of the system composed by 2 modules and characterized by 6 DoFs. The modal coupling locks the frequencies of one or several mode pairs at about the same value (light gray highlighted cells in Table 2); the real parts of the coalesced modes diverge towards opposite direction and one of the two becomes positive, i.e. unstable (dark gray highlighted cells).

	Friction coefficient μ													
	0.5		1.0		1.5		2.0		2.2		2.5		3.0	
Modes 1	-0.12	$\pm i36.55$	-0.14	$\pm i39.01$	-0.16	$\pm i41.39$	-0.18	$\pm i43.66$	-0.19	$\pm i44.62$	-0.20	$\pm i45.97$	-0.22	$\pm i48.21$
2	-0.41	$\pm i65.76$	-0.40	$\pm i65.54$	-0.40	$\pm i65.31$	-0.40	$\pm i65.08$	-0.40	$\pm i64.98$	-0.40	$\pm i64.84$	-0.39	$\pm i64.60$
3	-2.56	$\pm i164.77$	-2.59	$\pm i165.94$	-2.65	$\pm i167.70$	-4.57	$\pm i172.27$	-6.87	$\pm i171.88$	-8.76	$\pm i171.36$	-10.96	$\pm i170.52$
4	-3.20	$\pm i184.23$	-3.11	$\pm i181.62$	-3.00	$\pm i178.25$	-1.03	$\pm i172.38$	1.29	$\pm i172.14$	3.21	$\pm i171.75$	5.47	$\pm i171.05$
5	-4.46	$\pm i217.44$	-8.19	$\pm i219.61$	-10.32	$\pm i219.15$	-11.80	$\pm i218.76$	-12.34	$\pm i218.59$	-13.05	$\pm i218.35$	-14.11	$\pm i217.95$
6	-4.68	$\pm i222.79$	-0.91	$\pm i219.91$	1.24	$\pm i219.63$	2.75	$\pm i219.36$	3.32	$\pm i219.24$	4.04	$\pm i219.06$	5.14	$\pm i218.74$

$\lambda/2\pi$ [Hz]

Table 2: Real and imaginary part of the eigenvalues for several values of the friction coefficient, for the 2 module system. Dark-gray highlighted cell correspond to unstable modes while light-gray highlighted cells correspond to the coalesced modes.

Using the relations expressed in (32) and (33), it is possible to calculate $\widehat{P}_{m,r}$, the material dissipated power (35), associated to each modal contribution at the static equilibrium position. Table 3 shows this quantity calculated for each mode, for several values of the friction coefficient, in both stable and unstable conditions with one or more than one unstable modes. It is worth noting that, when two modes are coupled, the power dissipated by material damping on each mode is the same. This power can assume only positive values due to its nature of dissipative power (cf. (37)). Modes 3 and 4 show the highest values and the energy dissipated by these modes is several order of magnitude higher than the others, except that for the first mode.

	Friction coefficient μ						
	0.5	1.0	1.5	2.0	2.2	2.5	3.0
Modes 1	$4.54e+00$	$1.28e-01$	$5.91e-01$	$1.44e+00$	$1.90e+00$	$2.73e+00$	$4.54e+00$
2	$5.51e-10$	$7.74e-12$	$4.12e-11$	$1.17e-10$	$1.66e-10$	$2.68e-10$	$5.51e-10$
3	$3.41e+01$	$5.67e+00$	$2.05e+01$	$2.18e+02$	$6.33e+01$	$4.06e+01$	$3.41e+01$
4	$3.41e+01$	$1.01e+00$	$1.02e+01$	$2.18e+02$	$6.33e+01$	$4.06e+01$	$3.41e+01$
5	$9.77e-10$	$3.74e-10$	$4.84e-10$	$6.35e-10$	$7.00e-10$	$8.01e-10$	$9.77e-10$
6	$9.77e-10$	$3.74e-10$	$4.84e-10$	$6.35e-10$	$7.00e-10$	$8.01e-10$	$9.77e-10$

$\widehat{P}_{m,r}$ [W]

Table 3: Material dissipated power $\widehat{P}_{m,r}$ for several values of the friction coefficient. Highlighted cells corresponds to material dissipated power for coupled modes.

The power exchanged at the contact $\widehat{P}_{c,r}$ expressed in (36), for the same set of values of the friction coefficient, is reported in Table 4. In this case the sign of the power contribution depends to the phase difference between the tangential contact velocity and the tangential contact force at the different contact

points. It is positive if the power produces an increase of the mechanical energy of the system and it is negative otherwise. In this case, for the pair of coupled modes, the contact exchanged power assumes values with the same order of magnitude but opposite sign.

		Friction coefficient μ							
		0.5	1.0	1.5	2.0	2.2	2.5	3.0	
Modes	1	$-8.57e-05$	$-1.53e-02$	$-9.56e-02$	$-2.82e-01$	$-3.95e-01$	$-6.13e-01$	$-1.12e+00$	$\widehat{P}_{c,r}$ [W]
	2	$+2.31e-16$	$+5.33e-14$	$+4.30e-13$	$+1.66e-12$	$+2.60e-12$	$+4.79e-12$	$+1.20e-11$	
	3	$-1.21e-03$	$+4.76e-02$	$+4.08e-01$	$-1.50e+02$	$-9.35e+01$	$-8.88e+01$	$-1.03e+02$	
	4	$+7.51e-05$	$+2.25e-02$	$+3.23e-01$	$+1.64e+02$	$+9.74e+01$	$+9.10e+01$	$+1.04e+02$	
	5	$-3.91e-13$	$-2.98e-10$	$-6.16e-10$	$-1.02e-09$	$-1,21e-09$	$-1.51e-09$	$-2.07e-09$	
	6	$+7.38e-14$	$+3.02e-10$	$+6.13e-10$	$+1.01e-09$	$+1,19e-09$	$+1.48e-09$	$+2.03e-09$	

Table 4: Contact exchanged power $\widehat{P}_{c,r}$ for several values of the friction coefficient. Highlighted cells correspond to contact exchanged power for coupled modes, while, dark-gray highlighted cells correspond to unstable modes.

Finally, the MAI can be computed for each mode and its values are reported in the first part of Table 5, for the same set of values of the friction coefficient. The cells on Table 5 are light gray if the corresponding modes are coalesced, while they are dark gray highlighted if the corresponding mode is unstable. The bordered cells indicate the mode that is predicted to be unstable by the MAI.

The second part of Table 5 shows the values assumed by the eigenvalues real parts of the modes 4 and 6 that become unstable increasing the friction coefficient. Again, gray highlighted cells correspond to unstable modes, while bordered cells indicate the unstable mode with the highest value of the eigenvalue real part. Finally, the last part of the table shows the frequency actually recovered in the steady-state regime (limit-cycle) of the transient response f_{lc}, and the corresponding excited unstable mode.

The sign of the MAI results to be strictly related to the sign of the real part of the corresponding eigenvalues. Nevertheless, the respective value of MAI for the different unstable modes is not in agreement with the amplitude of the real part of the eigenvalues. In fact, being the magnitude of the powers that are involved in modes $3-4$ several order of magnitude higher than the ones of modes $5-6$ (cf. Table 4 and Table 3), when mode 4 becomes unstable ($\mathrm{Re}(\lambda_4) > 0$, for $\mu \geq 2.07$) the corresponding MAI value immediately overcomes the value of mode 6, i.e. the power absorption corresponding to the unstable pair of mode $3-4$ is larger.

In fact, this is in agreement with the actual unstable behavior of the system (cf. third part of Table 5) simulated by the transient analysis for the same values of the friction coefficient; as soon as the mode 4 is unstable ($\mathrm{Re}(\lambda_4) > 0$, for $\mu \geq 2.07$), the only frequency measured over the steady-state limit-cycle is 166Hz, which corresponds to the unstable mode 4.

On the contrary, the eigenvalues of the coalesced modes $5-6$ show an higher real part with respect to the modes $3-4$, for the same interval of the friction coefficient, which is not in agreement with the transient response of the system. The MAI index is able to predict the mode that will be at the origin of squeal vibrations in the transient behavior, when several modes are predicted to be unstable by CEA.

Figure 6(a) shows the transient response for a 2-modules system for a friction coefficient $\mu = 1.5$. For this value of the friction coefficient only the modes $5-6$ are coalesced and unstable. The mode predicted to be unstable both by the eigenvalue real part and by the Modal Absorption Index is the 6^{th} mode at a frequency of about 219 Hz (cf. Fig. 2). The frequency analysis (cf. Fig. 6(b)) of the response shows that during the linear phase, before the arising of contact status transitions ($0 < t < 0.7$s), during the saturation phase ($0.7 < t < 1.2$s) and during the steady-state regime ($2 < t < 3$s), the main frequency recovered is in agreement with the mode predicted to be unstable by both the eigenvalue real part and by the MAI.

For a friction coefficient $\mu = 2.2$ (cf. Table 5) the mode predicted to be unstable by the MAI is the 4^{th} mode, while by the analysis of the real parts of the eigenvalues the two coalesced couples of modes are both unstable, with positive real parts of the same order of magnitude and larger value for the 6^{th}. The comparison of these results with the transient response in Fig. 5(a) and its frequency analysis in Fig. 5(b), shows that the linear phase of the response ($0 < t < 0.25$s) and the saturation phase ($0.5 < t < 1.5$s) are characterized by the presence of both the unstable modes ($3-4$ and $5-6$ respectively at the frequency of

		Friction coefficient μ							
		0.5	1.0	1.5	2.0	2.2	2.5	3.0	
Modes	1	$-1.36e-03$	$-1.43e-01$	$-6.87e-01$	$-1.72e+00$	$-2.30e+00$	$-3.35e+00$	$-5.67e+00$	χ_r [W]
	2	$-6.80e-14$	$-7.69e-12$	$-4.07e-11$	$-1.16e-10$	$-1.64e-10$	$-2.63e-10$	$-5.39e-10$	
	3	$-2.27e+00$	$-5.62e+00$	$-2.01e+01$	$-3.68e+02$	$-1.57e+02$	$-1.29e+02$	$-1.37e+02$	
	4	$-6.44e-03$	$-9.83e-01$	$-9.88e+00$	$-5.42e+01$	$+3.41e+01$	$+5.04e+01$	$+7.03e+01$	
	5	$-2.58e-10$	$-6.72e-10$	$-1.10e-09$	$-1.66e-09$	$-1.91e-09$	$-2.31e-09$	$-3.05e-09$	
	6	$-7.92e-12$	$-7.23e-11$	$+1.30e-10$	$+3.76e-10$	$+4.91e-10$	$+6.82e-10$	$+1.05e-09$	
$\mathrm{Re}(\lambda_4/2\pi)$		-3.20	-3.11	-3.00	-1.03	$+1.29$	$+3.21$	$+5.47$	Hz
$\mathrm{Re}(\lambda_6/2\pi)$		-4.68	-0.91	$+1.24$	$+2.75$	$+3.32$	$+4.04$	$+5.14$	
f_{lc}		–	–	219	$219-166$	166	166	166	Hz
mode_{lc}		–	–	6	$6-4$	4	4	4	

Table 5: MAI index χ_r compared with the real part of complex eigenvalues for several values of the friction coefficient. Light-gray highlighted cells correspond to coupled modes, while dark-gray highlighted cells correspond to the unstable modes. f_{lc} is the frequency recovered in the steady-state limit-cycle during the transient analysis and mode_{lc} is the corresponding mode. Bordered values indicate the modes predicted to be unstable by the MAI index χ and by the real part of the eigenvalues.

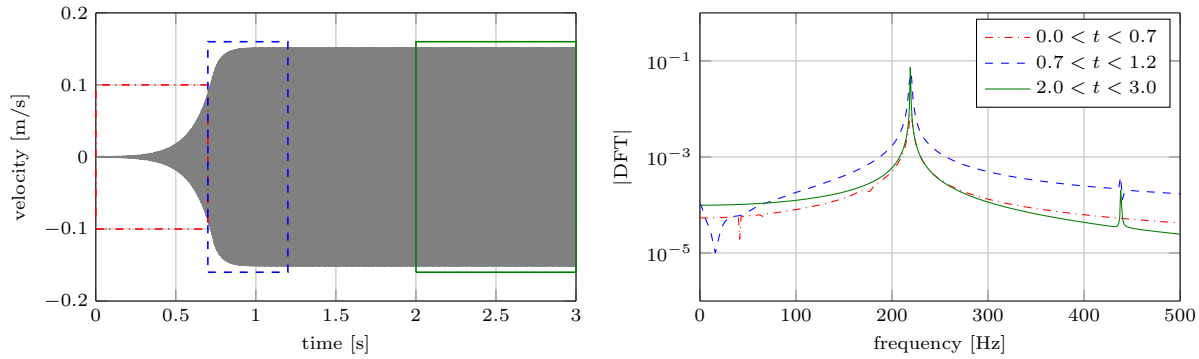

(a) Velocity response along x_1^1.

(b) Discrete Fourier Transform

Figure 6: Unstable transient response of a $N = 2$ system with friction coefficient $\mu = 1.5$.

166 Hz and 219 Hz). In particular, the amplitude of each mode contribution in the spectral analysis results to be strictly related to the shape of initial perturbation ε and to the value of the eigenvalue real parts (growth of vibration in linear phase). On the contrary, during the steady-state regime ($2 < t < 3$s), the only frequency detected is the one corresponding to the 4^{th} mode, as correctly predicted by the MAI (cf Table 5). While the transient linear increase of vibration is mainly affected by the different growth rate of the mode instabilities, when the nonlinearities excite the system at the contact interface, the MAI index indicates which mode will absorb more energy, i.e. will dominate the limit-cycle vibration.

5.2. Extension of the mode selection approach to more complex systems

In this section, the analysis is extended to a system composed by 4 modules to confirm the reliability of the approach showed in the previous section. The characteristic parameters of the system are the same as showed for the 2 modules system in Table 1.

Figure 7 shows the real and imaginary part of complex eigenvalue as a function of the friction coefficient. In this case the system has 12 DoFs and the complex modal analysis shows 24 complex and conjugated modes (cf. Fig. 7).

Due to the symmetry of the system there are double modes such as the mode $2, 3$ (at $f_{2,3} = 55$Hz for a nil friction coefficient) and modes $7, 8$ and $9, 10$ (respectively at $f_{7,8} = 191$Hz and $f_{9,10} = 206$Hz). Increasing the friction coefficient modes $5-6$, double modes $7, 8-9, 10$ and modes $11-12$ coalesce one each other and become unstable. The first coalescing modes are modes $11-12$ for a friction coefficient $\mu > 1.2$, and the system is unstable.

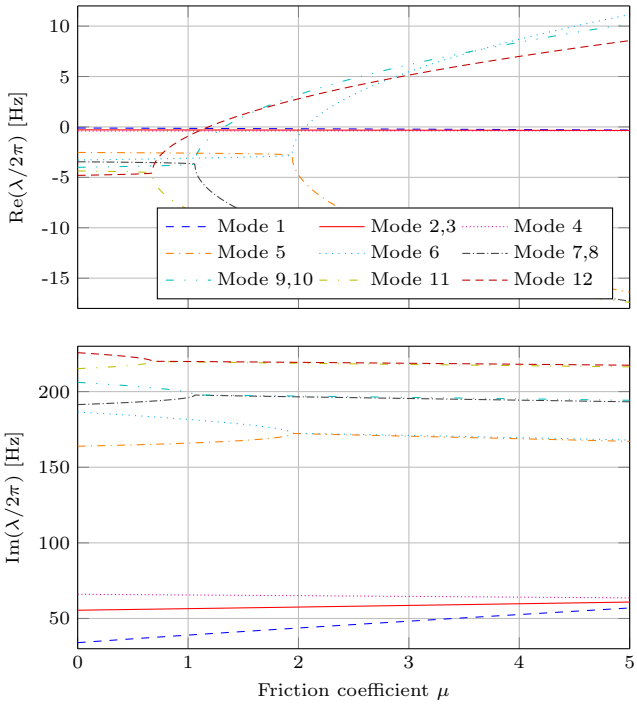

Figure 7: Real and Imaginary part of the complex eigenvalue λ as function of the friction coefficient μ for a system composed by 4 modules ($N = 4$)

Similarly to the 2 modules system, the MAI has been calculated for each mode and its values are shown in the first part of Table 6 for different values of the friction coefficient. Light gray highlighted cell indicate that modes are coalesced while dark gray highlighted cell indicate that the corresponding modes are unstable. Bordered cells indicate the unstable modes with the highest value of the MAI index, which are predicted to be the effectively squeal mode during the steady-state squeal vibrations.

The second part of Table 6 shows the values of eigenvalue real parts of the unstable modes of the 4 module system. Also in this case dark gray highlighted cells indicate that the corresponding modes are unstable. Bordered cells indicate the mode with the highest value of the eigenvalue real part, for each value of the friction coefficient.

Finally, the third part of Table 6 shows the main frequency f_{lc} recovered during the steady-state regime (limit-cycle) of the unstable response, and the corresponding unstable mode.

Also in this case the values assumed by the MAI highlight that there are some modes (1, 5 and 6 in Table 6) that, due to the decomposition of the static position on the modal base, are able to exchange an amount of energy that is several order of magnitude higher that the energy exchanged by the other modes. Since the mode with an higher real part of the eigenvalue is not always the mode recovered in the steady-state response of the system, the new index shows a better correspondence between the modes with highest MAI and the frequency recovered on the limit-cycle of the transient analysis (cf Table 6 and Fig. 8).

Furthermore, the analysis of the power flows around the equilibrium steady-state position, allows to better understand the presence of more frequencies in the steady-state response, observed sometime in the literature [15, 16, 37]. In fact, for specific values of the friction coefficient several mode frequencies are detected in the limit-cycle response; e.g. for a friction coefficient $\mu = 1.4$ there are two main peaks on the Discrete Fourier Transform of the steady-state response (red curve in Fig. 8) that correspond to modes $9 - 10$ and 12. The presence of several unstable mode in the steady-state response corresponds to values of the energy index of the same order of magnitude. When two unstable modes have similar capability to absorb energy from the contact, both of them can be present in the transient response.

		Friction coefficient μ						
		0.6	1.3	1.4	1.8	2.2	4.0	
Modes	1	$-3.73e-03$	$-8.31e-01$	$-1.08e+00$	$-2.49e+00$	$-4.59e+00$	$-2.58e+01$	χ_r[W]
	2,3	$-5.52e-13$	$-1.51e-10$	$-2.04e-10$	$-5.43e-10$	$-1.19e-09$	$-2.00e-08$	
	4	$-1.89e-13$	$-4.72e-11$	$-6.29e-11$	$-1.59e-10$	$-3.27e-10$	$-4.19e-09$	
	5	$-5.26e+00$	$-2.28e+01$	$-2.98e+01$	$-1.60e+02$	$-3.14e+02$	$-3.86e+02$	
	6	$-1.87e-02$	$-8.24e+00$	$-1.27e+01$	$-1.15e+02$	$+6.82e+01$	$+2.39e+02$	
	7,8	$-3.87e-09$	$-3.96e-08$	$-3.77e-08$	$-4.27e-08$	$-5.30e-08$	$-1.21e-07$	
	9,10	$-4.94e-11$	$-5.38e-10$	$+2.73e-09$	$+1.09e-08$	$+1.86e-08$	$+6.37e-08$	
	11	$-1.04e-09$	$-1.82e-09$	$-2.00e-09$	$-2.84e-09$	$-3.81e-09$	$-9.53e-09$	
	12	$-5.77e-11$	$+9.37e-11$	$+1.75e-10$	$+5.40e-10$	$+9.82e-10$	$+3.92e-09$	
$\mathrm{Re}(\lambda_6/2\pi)$		-20.00	-19.15	-19.01	-18.27	$+8.12$	$+54.61$	Hz
$\mathrm{Re}(\lambda_{9,10}/2\pi)$		-24.42	-1.29	$+2.87$	$+15.23$	$+24.44$	$+52.76$	
$\mathrm{Re}(\lambda_{12}/2\pi)$		-29.14	$+3.10$	$+5.55$	$+13.91$	$+20.84$	$+43.94$	
f_{lc}		–	220	195 – 219	168 – 195 – 219	166	166	Hz
mode_{lc}		–	12	9, 10 – 12	6 – 9, 10 – 12	6	6	

Table 6: MAI index χ_r compared with the real part of complex eigenvalues for several values of the friction coefficient. Light-gray highlighted cells correspond to the coalesced modes, while dark-gray highlighted cells correspond to the unstable modes. f_{lc} is the frequency recovered in the steady-state limit-cycle during the transient analysis and mode_{lc} is the corresponding mode. Bordered values correspond to the modes with highest value of the index χ and the eigenvalue real part.

When friction coefficient increases, the mode 6 becomes unstable and the steady-state is characterized by an harmonic behavior with only its frequency at $f = 166$Hz; this is due to the value of the energy index MAI, which becomes several order of magnitude greater than the others.

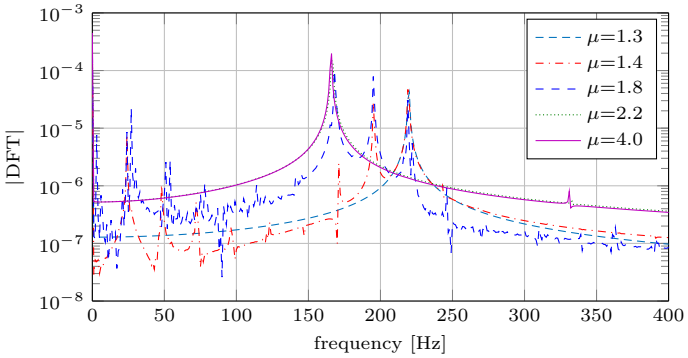

Figure 8: Discrete Fourier Transform of the steady-state limit-cycle for different values of friction coefficient.

Figure 8 shows the harmonic content of the steady-state transient response, for each value of the friction coefficient reported in Table 6. It shows how the MAI prediction is in very good agreement with the actual unstable transient response of the system.

5.3. Effect of the initial perturbation

Transient results showed in Section 5.1 and Section 5.2 are all obtained considering a small velocity perturbation ε in the x_1^1 direction. Therefore, the first part of the transient response is strictly related to the initial perturbation as well as to the eigenvalue real part.

Experimental observations and numerical analyses on extended mechanical systems show that the main frequency recovered during the linear phase of the response is generally characterized by the same modal frequency of the steady-state [17, 30, 36, 38]. This is due to the fact that for real frictional systems the perturbation comes from the contact interface and is generally related to the surface roughness and the local switch between contact states. Consequently, the initial perturbation is in this case a wide-band excitation acting at the contact interface. In order to reproduce this behavior, the same step variation of the speed

was applied to all the contact masses in the direction tangential to the contact. This produces a wide-band excitation that is geometrically distributed on the overall contact interface.

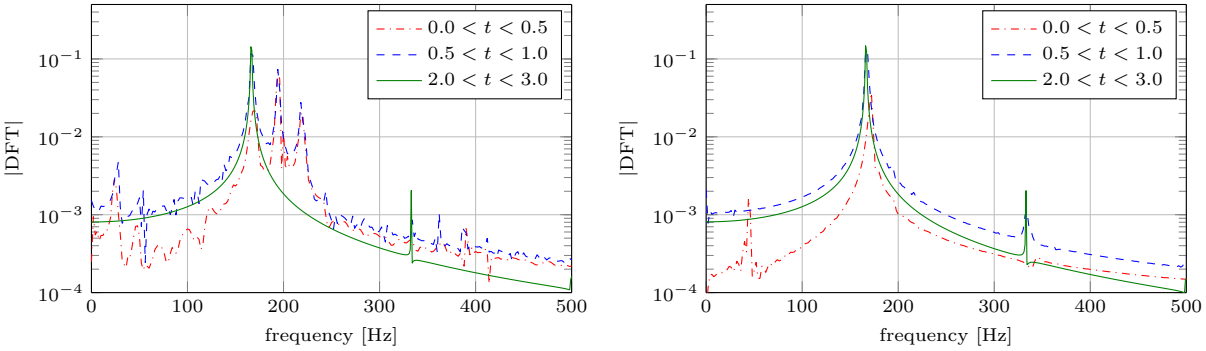

(a) Velocity perturbation on x_1^1 direction.

(b) Velocity perturbation on x_3^i directions.

Figure 9: Effect of the initial perturbation for a $N = 4$ system with a friction coefficient $\mu = 2.2$.

Figure 9 shows the harmonic content of the 4 modules system introduced in Section 5.2. In Fig. 9(a) the response is generated by a velocity perturbation ($\varepsilon = 1\text{e}-3\text{m/s}$) on the direction x_1^1, while, in Fig. 9(b) the response is generated by a perturbation applied on all the DoFs of the masses in contact along the direction parallel to the contact sliders x_3^i (cf. Fig. 1). The harmonic content of the initial phase ($0 < t < 0.5$), of the saturation phase ($0.5 < t < 1.0$) and of the steady-state limit-cycle ($2 < t < 3$) are shown. The comparison of these results highlight that while the initial response is affected by the initial perturbation, the response during the steady-state limit-cycle is always the same.

Due to the distribution of the perturbation at the contact interface, to be more representative of real perturbations on frictional systems, also the mode that is excited in the first phase of the simulation is the mode predicted by the MAI. In fact, the predicted mode has the highest capability to inject energy into the system from the contact interface, where the perturbation occurs.

6. Conclusions

In this paper a new instability index has been proposed to compare the different unstable modes recovered by CEA and to select the mode expected to become effectively unstable during the transient response of the system.

In order to test the index, a lumped model has been developed to reproduce the unstable friction induced vibrations. The stability of the system, as a function of the friction coefficient, has been presented both from a mathematical point of view, by the analysis of the eigenvalues, and from a physical point of view, by analyzing the power flows that the system exchanges with the environment during the friction-induced vibrations. The real part of the eigenvalues, even if it allows to indicate the stability of the system, is not generally useful as an indicator of the steady-state characteristics in case of multi-instability configuration.

The new stability index has been introduced by quantifying the capability of each mode to exchange energy with the external environment. The index is based on the projection of the static equilibrium position on the modal base, allowing to account for not only the sign of the energy content variation but also for the shape of the excitation source located at the contact. The broadband excitation coming from the frictional interface is more effective on the modes that have the highest level of local displacement and stresses at the contact. The projection on the initial condition allows for comparing the instability propensity of modes obtained by the CEA and defined with an arbitrary constant.

The analysis of the new energy index on the lumped system shows a good agreement between the steady-state response (unstable frequency) and the value of MAI index, compared among all the unstable system modes. Even when the magnitude of the real part of the eigenvalue is not in agreement with the transient unstable frequency, the mode predicted to absorb more energy by the MAI index generally corresponds

to the effective unstable frequency. Since the squeal is a highly nonlinear problem and the MAI index is computed starting from the linear conditions, some discordances can been observed when modes with similar values of the MAI index appear. The MAI index allows to define a hierarchy among the different system modes to better understand the evolution of the transient response up to the steady-state limit-cycle. The analysis of the MAI index allows as well to explain the appearance of squeal events with multiple unstable modes in the transient response, reported some times into the literature; mode with similar magnitude of the MAI index (absorbing energy capability) can coexist in the transient response.

Future work will be aimed to the extension of the presented approach to commercial brake systems using CEA by finite element codes, by calculating the MAI index from the system matrices and comparing the results with finite element transient analysis and experimental observations.

References

[1] A. Akay, Acoustics of friction, The Journal of the Acoustical Society of America 111 (4) (2002) 1525–1548. doi:10.1121/1.1456514.
URL http://link.aip.org/link/?JAS/111/1525/1

[2] R. A. Ibrahim, Friction-induced vibration, chatter, squeal, and chaos - part i: Mechanics of contact and friction, Applied Mechanics Reviews 47 (7) (1994) 209–226. doi:doi: 10.1115/1.3111079.
URL http://dx.doi.org/10.1115/1.3111079

[3] R. A. Ibrahim, Friction-induced vibration, chatter, squeal, and chaos - part ii: Dynamics and modeling, Applied Mechanics Reviews 47 (7) (1994) 227–253. doi:doi: 10.1115/1.3111080.
URL http://dx.doi.org/10.1115/1.3111080

[4] N. Kinkaid, O. O'Reilly, P. Papadopoulos, Automotive disc brake squeal, Journal of Sound and Vibration 267 (1) (2003) 105 – 166. doi:http://dx.doi.org/10.1016/S0022-460X(02)01573-0.
URL http://www.sciencedirect.com/science/article/pii/S0022460X02015730

[5] H. Ouyang, W. Nack, Y. Yuan, F. Chen, Numerical analysis of automotive disc brake squeal: a review, International Journal of Vehicle Noise and Vibration 1 (3-1) (2005) 207–231. doi:doi:10.1504/IJVNV.2005.007524.
URL http://www.ingentaconnect.com/content/ind/ijvnv/2005/00000001/F0020003/art00003

[6] C. Weiss, A. Hothan, G. Huber, M. M. Morlock, N. P. Hoffmann, Friction-induced whirl vibration: Root cause of squeaking in total hip arthroplasty, Journal of Biomechanics 45 (2) (2012) 297 – 303. doi:http://dx.doi.org/10.1016/j.jbiomech.2011.10.025.
URL http://www.sciencedirect.com/science/article/pii/S0021929011006671

[7] G. Ouenzerfi, F. Massi, E. Renault, Y. Berthier, Squeaking friction phenomena in ceramic hip endoprosthesis: Modeling and experimental validation, Mechanical Systems and Signal Processing 58 - ??59 (0) (2015) 87 – 100. doi:http://dx.doi.org/10.1016/j.ymssp.2014.09.012.
URL http://www.sciencedirect.com/science/article/pii/S0888327014004713

[8] G. Chen, Z. Zhou, Correlation of a negative friction velocity slope with squeal generation under reciprocating sliding conditions, Wear 255 (2003) 376 – 384, 14th International Conference on Wear of Materials. doi:http://dx.doi.org/10.1016/S0043-1648(03)00052-8.
URL http://www.sciencedirect.com/science/article/pii/S0043164803000528

[9] H. Ouyang, J. Mottershead, M. Cartmell, M. Friswell, Friction-induced parametric resonances in discs: effect of a negative friction-velocity relationship, Journal of Sound and Vibration 209 (2) (1998) 251 – 264. doi:http://dx.doi.org/10.1006/jsvi.1997.1261.
URL http://www.sciencedirect.com/science/article/pii/S0022460X9791261X

[10] R. T. Spurr, A theory of brake squeal, Proceedings of the Institution of Mechanical Engineers: Automobile Division 15 (1) (1961) 33–52.

[11] M. North, Disc brake squeal: a theoretical model, Hillington Press, 1972.

[12] R. D. Blevins, Flow-induced vibration, New York, Van Nostrand Reinhold Co., 1977. 377 p. 1.

[13] J.-J. Sinou, F. Thouverez, L. Jézéquel, Methods to reduce non-linear mechanical systems for instability computation, Archives of Computational Methods in Engineering 11 (3) (2004) 257–344. doi:10.1007/BF02736228.
URL http://dx.doi.org/10.1007/BF02736228

[14] J.-J. Sinou, F. Thouverez, L. Jézéquel, Stability analysis and non-linear behaviour of structural systems using the complex non-linear modal analysis (cnlma), Computers & Structures 84 (29-30) (2006) 1891 – 1905. doi:http://dx.doi.org/10.1016/j.compstruc.2006.08.020.
URL http://www.sciencedirect.com/science/article/pii/S0045794906002501

[15] J.-J. Sinou, N. Coudeyras, S. Nacivet, Study of the nonlinear stationary dynamic of single and multi-instabilities for disk brake squeal, International Journal of Vehicle Design 51 (1-2) (2009) 207–222.

[16] F. Chevillot, J.-J. Sinou, N. Hardouin, Nonlinear transient vibrations and coexistences of multi-instabilities induced by friction in an aircraft braking system, Journal of Sound and Vibration 328 (2009) 555 – 574. doi:http://dx.doi.org/10.1016/j.jsv.2009.08.028.
URL http://www.sciencedirect.com/science/article/pii/S0022460X09006865

[17] J. Brunetti, F. Massi, A. Saulot, M. Renouf, W. D'Ambrogio, System dynamic instabilities induced by sliding contact: A numerical analysis with experimental validation., Mechanical Systems and Signal Processings 58-59 (2015) 70–86. doi:10.1016/j.ymssp.2015.01.006.
URL http://www.sciencedirect.com/science/article/pii/S0888327015000084

[18] D. Guan, J. Huang, The method of feed-in energy on disc brake squeal, Journal of Sound and Vibration 261 (2) (2003) 297 – 307. doi:http://dx.doi.org/10.1016/S0022-460X(02)01074-X.
URL http://www.sciencedirect.com/science/article/pii/S0022460X0201074X

[19] J. F. Tarter, Prediction of unstable friction-induced vibrations using an energy criterion, Ph.D. thesis, Carnegie Mellon University (2004).

[20] T. Irvine, Effective modal mass and modal participation factors, Available on the web on site: http://www. vibrationdata. com/tutorials2/ModalMass. pdf.(last access on march 7 2007).

[21] G. G. Adams, Steady sliding of two elastic half-spaces with friction reduction due to interface stick-slip, Journal of Applied Mechanics 65 (2) (1998) 470–475. doi:doi: 10.1115/1.2789077.
URL http://dx.doi.org/10.1115/1.2789077

[22] G. G. Adams, Self-excited oscillations of two elastic half-spaces sliding with a constant coefficient of friction, Journal of Applied Mechanics 62 (4) (1995) 867–872. doi:doi: 10.1115/1.2896013.
URL http://dx.doi.org/10.1115/1.2896013

[23] L. Baillet, S. D'Errico, Y. Berthier, Influence of sliding contact local dynamics on macroscopic friction coefficient variation, Revue Européenne des Éléments finis 14 (2-3) (2005) 305–321. arXiv:http://www.tandfonline.com/doi/pdf/10.3166/reef.14.305-321, doi:10.3166/reef.14.305-321.
URL http://www.tandfonline.com/doi/abs/10.3166/reef.14.305-321

[24] E. Chatelet, G. Michon, L. Manin, G. Jacquet, Stick/slip phenomena in dynamics: Choice of contact model. numerical predictions & experiments, Mechanism and Machine Theory 43 (10) (2008) 1211 – 1224. doi:http://dx.doi.org/10.1016/j.mechmachtheory.2007.11.001.
URL http://www.sciencedirect.com/science/article/pii/S0094114X07001723

[25] M. Di Bartolomeo, F. Massi, L. Baillet, A. Culla, A. Fregolent, Y. Berthier, Wave and rupture propagation at frictional bimaterial sliding interfaces: From local to global dynamics, from stick-slip to continuous sliding, Tribology International 52 (0) (2012) 117 – 131. doi:http://dx.doi.org/10.1016/j.triboint.2012.03.008.
URL http://www.sciencedirect.com/science/article/pii/S0301679X12001053

[26] N. Hoffmann, M. Fischer, R. Allgaier, L. Gaul, A minimal model for studying properties of the mode-coupling type instability in friction induced oscillations, Mechanics Research Communications 29 (4) (2002) 197 – 205. doi:http://dx.doi.org/10.1016/S0093-6413(02)00254-9.
URL http://www.sciencedirect.com/science/article/pii/S0093641302002549

[27] F. Massi, J. Rocchi, A. Culla, Y. Berthier, Coupling system dynamics and contact behaviour: Modelling bearings subjected to environmental induced vibrations and "false brinelling" degradation, Mechanical Systems and Signal Processing 24 (4) (2010) 1068 – 1080. doi:http://dx.doi.org/10.1016/j.ymssp.2009.09.004.
URL http://www.sciencedirect.com/science/article/pii/S0888327009002647

[28] M. Renouf, F. Massi, A. Saulot, N. Fillot, Numerical tribology of dry contact, Tribology International 44 (7-8) (2011) 834–844.

[29] J.-J. Sinou, L. Jézéquel, Mode coupling instability in friction-induced vibrations and its dependency on system parameters including damping, European Journal of Mechanics - A/Solids 26 (1) (2007) 106 – 122. doi:http://dx.doi.org/10.1016/j.euromechsol.2006.03.002.
URL http://www.sciencedirect.com/science/article/pii/S099775380600026X

[30] D. Tonazzi, F. Massi, A. Culla, L. Baillet, A. Fregolent, Y. Berthier, Instability scenarios between elastic media under frictional contact, Mechanical Systems and Signal Processing 40 (2) (2013) 754 – 766. doi:http://dx.doi.org/10.1016/j.ymssp.2013.05.022.
URL http://www.sciencedirect.com/science/article/pii/S0888327013002811

[31] V. Linck, L. Baillet, Y. Berthier, Dry friction: influence of local dynamic aspect on contact pressure, kinematics and friction, in: D. D. G. Dalmaz, A.A. Lubrecht, M. Priest (Eds.), Transient Processes in Tribology Proceedings of the 30th Leeds-Lyon Symposium on Tribology, Vol. 43 of Tribology Series, Elsevier, 2003, pp. 545 – 552. doi:http://dx.doi.org/10.1016/S0167-8922(03)80082-2.
URL http://www.sciencedirect.com/science/article/pii/S0167892203800822

[32] J. Brunetti, F. Massi, W. D'Ambrogio, Y. Berthier, Dynamic and energy analysis of frictional contact instabilities on a lumped system, Meccanica 50 (3) (2015) 633–647. doi:10.1007/s11012-014-0020-0.
URL http://dx.doi.org/10.1007/s11012-014-0020-0

[33] J. Brunetti, F. Massi, W. D'Ambrogio, L. Baillet, Steady state of modal coupling instabilities as a dynamic energy equilibrium, in: Proceeding of ISMA2014 including USD2014, 2014.

[34] F. Massi, O. Giannini, Effect of damping on the propensity of squeal instability: An experimental investigation, The Journal of the Acoustical Society of America 123 (4) (2008) 2017–2023. doi:10.1121/1.2875628.
URL http://link.aip.org/link/?JAS/123/2017/1

[35] F. Massi, L. Baillet, O. Giannini, A. Sestieri, Brake squeal: Linear and nonlinear numerical approaches, Mechanical Systems and Signal Processing 21 (6) (2007) 2374 – 2393. doi:http://dx.doi.org/10.1016/j.ymssp.2006.12.008.
URL http://www.sciencedirect.com/science/article/pii/S0888327007000039

[36] F. Massi, O. Giannini, L. Baillet, Brake squeal as dynamic instability: An experimental investigation, The Journal of the Acoustical Society of America 120 (3) (2006) 1388–1398. doi:10.1121/1.2228745.

URL http://link.aip.org/link/?JAS/120/1388/1
[37] N. Coudeyras, S. Nacivet, J.-J. Sinou, Periodic and quasi-periodic solutions for multi-instabilities involved in brake squeal, Journal of Sound and Vibration 328 (4-5) (2009) 520–540. doi:http://dx.doi.org/10.1016/j.jsv.2009.08.017.
URL http://www.sciencedirect.com/science/article/pii/S0022460X09006609
[38] F. Massi, O. Giannini, et al., Extension of a modal instability theory to real brake systems, in: Proc. International Modal Analysis Conference-IMAC-XXIII, Orlando, Florida, 2005.